Multidisciplinary and Multifidelity Design Optimization of Electric Vehicle Battery Thermal Management System

Xiaobang Wang
School of Mechanical Engineering,
Dalian University of Technology,
Dalian 116024, LN, China;
Department of Mechanical Engineering,
The University of Texas at Dallas,
Richardson, TX 75080
e-mail: wxbang@mail.dlut.edu.cn

Yuanzhi Liu
Department of Mechanical Engineering,
The University of Texas at Dallas,
Richardson, TX 75080
e-mail: yuanzhi.liu@utdallas.edu

Wei Sun
School of Mechanical Engineering,
Dalian University of Technology,
Dalian 116024, LN, China
e-mail: sunwei@dlut.edu.cn

Xueguan Song
School of Mechanical Engineering,
Dalian University of Technology Dalian,
Dalian 116024, LN, China
e-mail: sxg@dlut.edu.cn

Jie Zhang[1]
Department of Mechanical Engineering,
The University of Texas at Dallas,
Richardson, TX 75080
e-mail: jiezhang@utdallas.edu

Battery thermal management system (BTMS) is a complex and highly integrated system, which is used to control the battery thermal conditions in electric vehicles (EVs). The BTMS consists of many subsystems that belong to different disciplines, which poses challenges to BTMS optimization using conventional methods. This paper develops a general variable fidelity-based multidisciplinary design optimization (MDO) architecture and optimizes the BTMS by considering different systems/disciplines from the systemic perspective. Four subsystems and/or subdisciplines are modeled, including the battery thermodynamics, fluid dynamics, structure, and lifetime model. To perform the variable fidelity-based MDO of the BTMS, two computational fluid dynamics (CFD) models with different levels of fidelity are developed. A low fidelity surrogate model and a tuned low fidelity model are also developed using an automatic surrogate model selection method, the concurrent surrogate model selection (COSMOS). An adaptive model switching (AMS) method is utilized to realize the adaptive switch between variable-fidelity models. The objectives are to maximize the battery lifetime and to minimize the battery volume, the fan's power, and the temperature difference among different cells. The results show that the variable-fidelity MDO can balance the characteristics of the low fidelity mathematical models and the computationally expensive simulations, and find the optimal solutions efficiently and accurately. [DOI: 10.1115/1.4040484]

Keywords: battery thermal management system, variable-fidelity optimization, multidisciplinary design optimization, electric vehicle

1 Introduction

Electric vehicles (EVs) have been developing rapidly in recent years. As a core component, the battery package is the only power source for the whole EV system. Due to many excellent properties, such as the high voltage and no memory effect, the lithium-ion battery is currently one of the most widely used batteries in EVs. Nevertheless, potential issues of the lithium-ion battery, such as the overtemperature and the overcharge/overdischarge, may lead to a life-threatening explosion. To address these thermal issues, different types of battery thermal management systems (BTMS) have been developed. As an integrated component, the BTMS is usually embedded into the battery, which leads to many subsystems belonging to different disciplines being coupled with each other in a small space. Thus, optimizing a single discipline may not meet the practical engineering requirements. In this paper, we develop a variable fidelity-based multidisciplinary design optimization (MDO) method to optimize the BTMS, which models and solves the multiple systems/disciplines problem from the systemic level.

1.1 Lithium-Ion Battery Thermal Management System. Among different types of BTMS (e.g., air cooling, forced convective liquid cooling, heat pipe, and phase change material), the air-based BTMS has the advantages of low cost structure and light weight. Various methods have been developed in the literature to study the air-based BTMS, including numerical simulations, experiments, and optimization. Most of the existing work in air-based BTMS focuses on the cooling channel design and optimization. For example, Park [1] simulated the cooling performance with different types of air ventilations, and found that the cooling performance was significantly improved by adding an extra ventilation. Xun et al. [2] developed numerical models for BTMS to analyze the impacts of the volume ratio and the size of the cooling channel, and found that a larger channel could improve the evenness of the temperature distribution and the energy efficiency. Other work focused on adding auxiliary components to enhance the heat transfer for air-based BTMS. For example, Sun and Dixon [3] developed a transient battery thermal model and proposed a "Z-type" air-cooled battery pack with taper manifold, cooling plate, and corrugations to improve the battery temperature uniformity. Mohammadian and Zhang [4] embedded metal foam and pin-fin heat sinks to an air-cooled battery to enhance the thermal performance.

For the design optimization of air-based BTMS, Uddin and Ku [5] designed and analyzed an air-based BTMS through a three-dimensional computational fluid dynamics (CFD) modeling approach and the results showed that the maximum temperature gradient within each cell was minimized to be 1.4 °C. Dandurand et al. [6] proposed a multi-objective optimization model which minimized cell temperature deviations while maintaining evenness of temperature distribution of an air-based BTMS.

1.2 Variable-Fidelity Optimization. Most of existing literature focuses on the BTMS from a single discipline/subsystem, rather than a global and systematic point of view. Due to the complex coupling effects among the whole system, this individual discipline study on the BTMS may overemphasize a single

[1]Corresponding author.

Contributed by the Design Automation Committee of ASME for publication in the Journal of Mechanical Design. Manuscript received August 19, 2017; final manuscript received May 24, 2018; published online June 22, 2018. Assoc. Editor: Gary Wang.

subsystem/discipline while neglect other key subsystems/disciplines. In addition, the uncertain inaccuracy of the pure mathematical models and the expensive computation of the simulation analysis can both lead to some corresponding demerits for the design and optimization of the BTMS. To this end, a variable fidelity-based MDO method is developed and applied to BTMS in this paper to design and optimize different BTMS subsystems simultaneously, by integrating the merits of the pure mathematical models and the expensive computational simulations.

The variable fidelity (multifidelity)-based design optimization strategy has been widely used to improve the computational efficiency and accuracy for the design of complex engineering systems. For example, Mejía-Rodríguez et al. [7] developed a variable fidelity material design methodology to integrate material performance analyses with differing levels of fidelity using a model management framework. Xiong et al. [8] proposed a new variable-fidelity optimization approach from the perspective of reducing the uncertainty of using surrogate models in engineering design based on model fusion and objective-oriented sequential sampling. Yamazaki and Mavriplis [9] utilized the Co-Kriging method to develop a derivative-enhanced variable-fidelity surrogate model, based on which the aerodynamic shape optimization was conducted. Rethore et al. [10] applied a variable-fidelity approach to perform a layout optimization for an offshore wind farm to accelerate the convergence speed.

The remainder of the paper is organized as follows: Section 2 establishes the general variable fidelity-based MDO architecture and the detailed corresponding configurations. Section 3 constructs the variable-fidelity models, including the high fidelity CFD models, the tuned low fidelity models, and the low fidelity surrogate models. In Sec. 4, the variable fidelity-based MDO of BTMS is developed and the optimization results are obtained. Section 5 provides the concluding remarks and future work.

2 Variable Fidelity-Based Multidisciplinary Design Optimization Architecture

2.1 Overall Architecture. There have been many MDO architectures proposed in the literature to deal with the multidisciplinary coupling optimization problems, such as the multidisciplinary feasible (MDF) and the collaborative optimization. These MDO architectures are generally applied to computationally expensive high fidelity simulations or low fidelity physical models (or surrogate models) [11,12]. With the aim of finding the trade-off between computational time and accuracy when solving complex engineering systems, a variable fidelity-based MDO architecture is proposed in this paper by integrating the conventional MDO architectures and model switching techniques, as illustrated in Fig. 1.

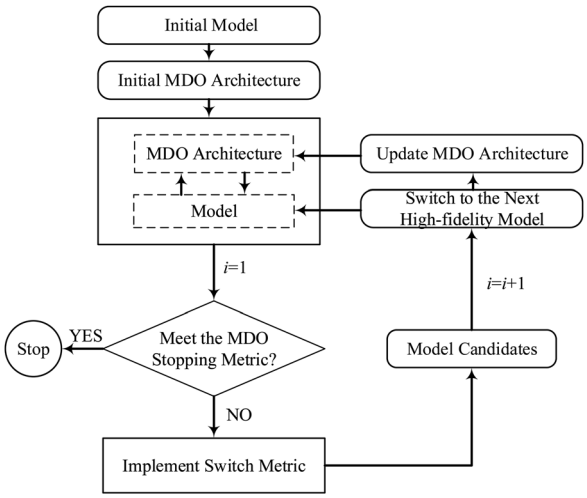

Fig. 2 An overall flow chart of the variable-fidelity-based MDO process

As seen from Fig. 1, the variable fidelity-based MDO process consists of $n+1$ optimization stages, including n mathematical model stages and a high fidelity numerical simulation model stage, and a model with a specific level of fidelity is used in each stage to perform the optimization. The models with different levels of fidelity are defined as the variable-fidelity models, where the computational cost of the model is generally related to the accuracy of the model estimation [13]. Each variable-fidelity model can be either a physics-based model or a nonphysics-based model (e.g., surrogate model and tuned low fidelity model). The numerical simulation model established by tools such as ANSYS and ABAQUS is considered as the highest fidelity model in the developed variable fidelity-based MDO process. Figure 2 illustrates the overall process of the proposed method. First, an initial MDO architecture and models are selected to start the multifidelity MDO process. During the MDO process, a switch metric is

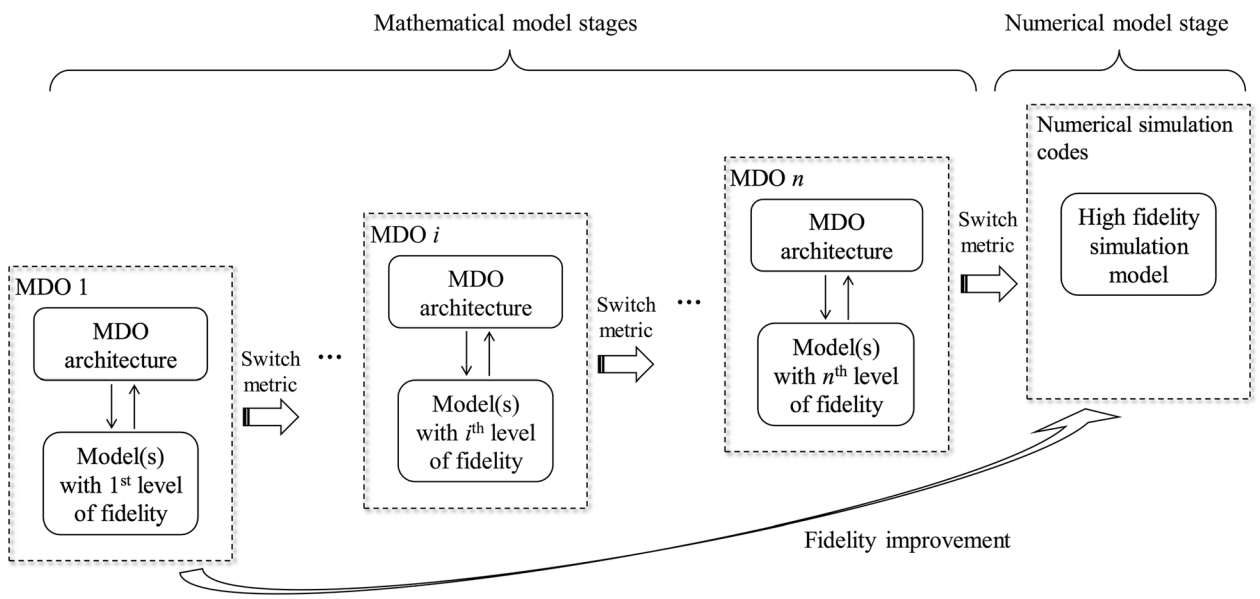

Fig. 1 Variable fidelity-based MDO architecture

used and evaluated at every optimization iteration. If the switching criterion is met, the optimization process will switch to the next MDO stage with a higher level of fidelity model and an updated MDO architecture. Or else, the optimization will continue with the next iteration in the current MDO stage. It should be noted that the optimization process can terminate and obtain the final optimal function value at any time, if the iteration process satisfies the MDO stopping criterion.

Different switch metrics can be used based on the characteristics of the problem, such as the expected improvement criterion [14], trust-region methods [15], and adaptive model switching (AMS) [13].

2.2 Adaptive Model Switching. In this paper, the AMS method is adopted to perform the multifidelity-based MDO of BTMS. Compared with the expected improvement criterion, trust-region methods, and some other switching methods, the AMS can be coherently applied to different types of low fidelity models and allows an adaptive switching among multiple models [13]. The switching metric of the AMS method is based on whether the uncertainty associated with the current model output dominates the latest improvement of the relative fitness function [13]. The switching principle of AMS metric is illustrated in Fig. 3, where the dashed curve with the shared area represents the current model error distribution and the two solid curves represent the distributions of the relative fitness function improvement in different iterations during the optimization process. It is noted that all the distributions used in AMS of this paper are estimated by log-normal distributions using the predictive estimation of model fidelity method [16]. The parameter e_m is the global model error and the corresponding critical probability $p_{\rm cr}$ is the critical bound in the error distribution of the current model. The parameters $e_{\rm f1}$ and $e_{\rm f2}$ are the precomputed cut-off values in the distributions of fitness function improvement. If the current model error, e_m, is greater than the precomputed cut-off value, e_{f1}, the optimization process will switch to the next higher fidelity model. And if the current model error, e_m, is less than the precomputed cut-off value, e_{f2}, the optimization process will stay and use the current model to conduct the next optimization iteration. The critical probability, $p_{\rm cr}$, can be defined by the engineers based on the specific optimization problems.

In this paper, we have adopted and also extended the AMS technique to be more generic. The original AMS technique is restricted to be used with the population-based optimization algorithms (e.g., genetic algorithm and particle swarm optimization) and uses the entire population to construct the distribution of the relative fitness function improvement. In this paper, the relative fitness function improvement obtained from a series of individual optimization iterations can also be used to construct the corresponding distributions. Therefore, the AMS technique can be used with any optimization algorithm by selecting appropriate establishment methods for the distribution of the relative fitness function improvement.

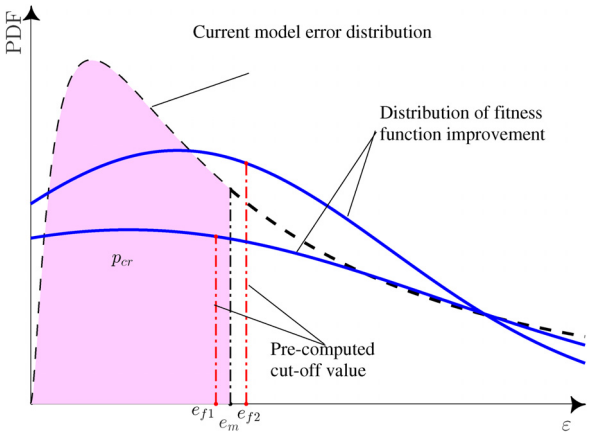

Fig. 3 The switching metric of the AMS. PDF: probability density function.

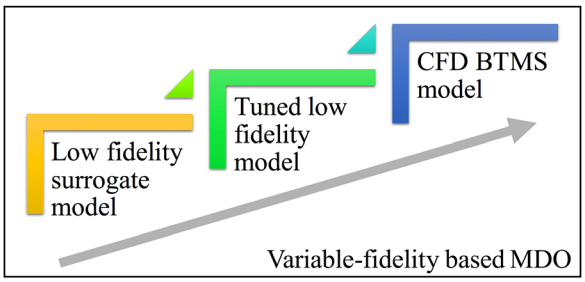

Fig. 4 Variable-fidelity models for the BTMS

3 Variable-Fidelity Models Establishment

Battery thermal management system is a complex system that consists of many modules belonging to different disciplines [17]; therefore, a corresponding multidisciplinary analysis of the BTMS should be conducted beforehand when the variable-fidelity models are established. In this paper, four subsystems/disciplines are taken into account, including the battery thermodynamic, fluid dynamic (air), lifetime, and structure. More details on the disciplines selection and multidisciplinary analysis of BTMS can be found in Ref. [17].

In this paper, three types of BTMS models with different levels of fidelity are used to perform the variable-fidelity optimization as illustrated in Fig. 4. The models rank from low to high as the low fidelity surrogate model, the tuned low fidelity model, and the high fidelity CFD model.

3.1 High Fidelity Computational Fluid Dynamics Model. Both the tapered manifold shape and the uneven passage spacing size are taken into account in the modeling and optimization of this paper. Figure 5 shows an air-based BTMS model with a lithium-ion battery module, which contains ten lithium-ion prismatic cells (65 mm × 151 mm × 16 mm) unevenly distributing in the package. In this "U" type battery module, the cooling air steam is pumped from the inlet at the bottom left by the fan, passes through the 11 passages, and then outflows through the outlet at the top left. From the left to the right, the cells and the passages are numbered from small to large, as illustrated in Fig. 5, where $b_1 \sim b_{11}$ denote the passage spacing size. The inlet and outlet manifolds are tapered and the taper is determined by the external size a_1, a_2 and inner size a_3, a_4.

In order to simulate the working environment, the lithium-ion battery is assumed to work under the most common conditions with the air temperature being 20 °C. In the meanwhile, the heat flux, $\dot{q}$ (W/m^2), is assumed to be only generated uniformly on the

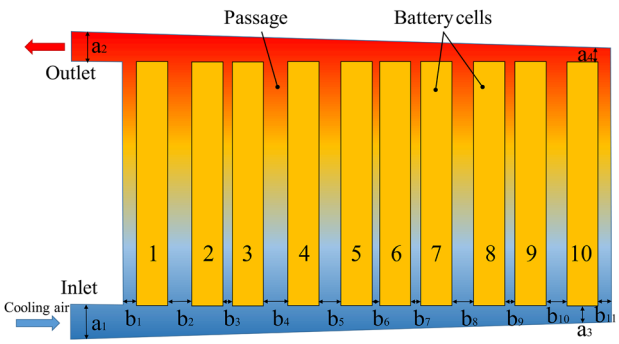

Fig. 5 A ten battery cell air-based BTMS model

Table 1 Upper and lower bounds of design variables

Design parameter (unit)	Lower bound	Upper bound
$b_{1\sim11}$ (mm)	0.500	5.000
$a_{1\sim4}$ (mm)	3.000	15.000
$\dot{m}$ (kg/s)	0.001	0.020
$\dot{q}$ (W/m^2)	200.000	350.000

Table 2 The configurations of the low fidelity surrogate models

Model	Model type	Kernel function	Hyper-parameter	Error criterion
$T_{\max}$	SVR	RBF	$\gamma = 38.20$ $C = 0.7268$	$e_{\text{med}} = 0.2482$ $e_{\max} = 0.6314$
ΔT	SVR	Linear	$C = 0.1890$	$e_{\text{med}} = 0.2443$ $e_{\max} = 0.5255$
Δp	RBF	Gaussian	$\sigma = 0.1364$	$e_{\text{med}} = 0.1234$ $e_{\max} = 0.4242$

surfaces of the battery cells. A total of 17 key parameters are selected as the design variables: the passage spacing size $b_{1\sim11}$ (mm), the air manifold size $a_{1\sim4}$ (mm), the mass flow rate of the cooling air, $\dot{m}$ (kg/s), and the heat flux from the battery cell to the air, $\dot{q}$ (W/m^2). Based on the physical structure characteristics and the performance requirement, corresponding boundaries of key parameters to conduct CFD are listed in Table 1. In this paper, the commercial software ANSYS 17.1 is utilized to build the CFD model. The CFD mesh is constructed using quadrangular cells, characterized by 871,038 quadrangular cells and 767,250 grid points.

3.2 Low Fidelity Surrogate Models. From the multidisciplinary analysis [17], the average temperature, $T_{\max}$ (°C), the maximum temperature difference, ΔT (°C), and the pressure drop, Δp (Pa), are selected as the outputs. To build the low fidelity surrogate models, the Sobol sequence [18] is used to generate 200 training points. The high fidelity CFD model built in Sec. 3.1 is utilized to perform the design of experiments (DoE). For the surrogate models, different combinations of model types (including radial basis function (RBF), Kriging, support vector regression (SVR), etc.), kernel functions (including Linear, Cubic, Gaussian, etc.), and hyper-parameters can lead to different accuracies. Aiming to find the most suitable surrogate models, the concurrent surrogate model selection (COSMOS) method [17] is adopted to automatically determine the specific configurations of surrogate models for the variable-fidelity modeling. By using COSMOS, the selected best configurations of the low fidelity surrogate models, including $T_{\max}$, ΔT, and ΔT, are listed in Table 2.

By using the log-normal distribution, the distributions of errors in the low fidelity surrogate models of $T_{\max}$, ΔT, and Δp are illustrated in Fig. 6. Based on the numerical experiments conducted in Sec. 4.3, the critical bound of the error distribution p_{cr} is set to be 0.05 in this paper, so the global model errors of the three low fidelity surrogate models can be obtained as $e_{m_{\Delta p}} = 0.0704$, $e_{m_{\Delta T}} = 0.1261$, and $e_{m_{T_{\max}}} = 0.1288$. Given that three surrogate models existing simultaneously in a single computing phase, the AMS metric in this paper is determined based on the current surrogate model with the largest global model error. Thus, the surrogate of $T_{\max}$ is used to identify the AMS metric, since it presents the largest error of 0.1288.

3.3 Tuned Low Fidelity Models. The tuned low fidelity model is a high-quality hybrid approximation model, which has a similar level of accuracy as the high fidelity model but at the same

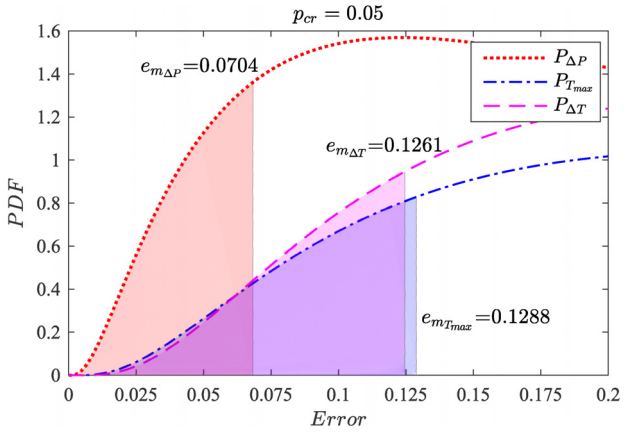

Fig. 6 Distributions of errors in the low fidelity surrogate models of $T_{\max}$, ΔT, and Δp

Table 3 The configurations of the tuned low fidelity models

Model	Model type	Kernel function	Hyper-parameter	Error criterion
$T_{\max}$	SVR	Linear	$C = 0.9505$	$e_{\text{med}} = 0.1349$ $e_{\max} = 0.3510$
ΔT	SVR	Linear	$C = 0.4424$	$e_{\text{med}} = 0.2217$ $e_{\max} = 0.5670$
Δp	RBF	Gaussian	$\sigma = 0.0899$	$e_{\text{med}} = 0.1131$ $e_{\max} = 0.6107$

time remains a computationally inexpensive model [19]. There are two ways to establish the tuned low fidelity models using the interaction between low and high fidelity models [20,13]: the multiplicative method and the additive method. In this paper, the multiplicative method is adopted to construct the tuned low fidelity models for $T_{\max}$, ΔT, and Δp. By generating 200 low fidelity points through a low fidelity CFD model of BTMS with 340,929 quadrangular cells and 288,332 grid points, a tuned low fidelity model can be established. By using COSMOS, the selected best configurations of tuned low fidelity models, including $T_{\max}$, ΔT, and ΔT, are listed in Table 3.

The log-normal distributions of errors in the tuned low fidelity models of $T_{\max}$, ΔT, and Δp are illustrated in Fig. 7. By setting p_{cr} to be 0.05, the global model errors of the three tuned low fidelity surrogate models are $e_{m_{\Delta p}} = 0.0721$, $e_{m_{\Delta T}} = 0.1152$, and $e_{m_{T_{\max}}} = 0.0680$. So, as mentioned in Sec. 3.2, in this optimization

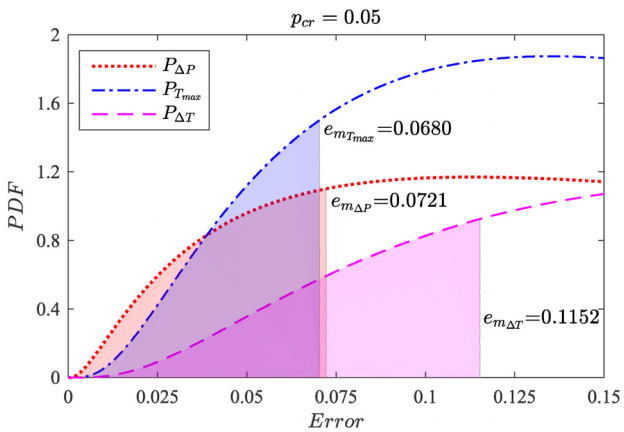

Fig. 7 Distributions of error in the tuned low fidelity models of $T_{\max}$, ΔT, and Δp

phase, the tuned low fidelity model of ΔT is selected to identify the AMS metric.

4 Variable Fidelity-Based Multidisciplinary Design Optimization of Battery Thermal Management System

4.1 Multidisciplinary Design Optimization Establishment. As noted above, 17 design variables are selected as shown in the following equation:

$$\mathbf{X} = [x_1, x_2, \ldots, x_{17}] = [b_{1\sim11}, a_{1\sim4}, \dot{q}, \dot{m}] \tag{1}$$

The lower and upper bounds of the 17 design variables are listed in Table 1. Based on the multidisciplinary analysis of BTMS and the variable-fidelity models built in Sec. 3, the overall MDO of the BTMS is modeled as below:

$$\begin{cases} \text{find} & \mathbf{X} = [x_1, x_2, \ldots, x_{17}] \\ \min & f = \left(\frac{1}{t}\right)^{\lambda_1} \cdot \Delta T^{\lambda_2} \cdot P_F^{\lambda_3} \cdot V^{\lambda_4} \\ \text{s.t.} & g_i \le 0 \quad (i = 1, 2, 3, 4, 5, 6) \\ & \Delta p = f([x_1, x_2, \ldots, x_{17}]) \\ & x_{16} = \xi \dfrac{\Delta p \cdot x_{17}}{36 A \rho \eta} + \dot{q}_v \end{cases} \tag{2}$$

The optimization objective is composed of four parts, including maximizing the battery lifetime t (year), minimizing temperature difference ΔT (°C), minimizing the power consumed by the fan P_F (W), and minimizing the volume of the battery V (m^3). A weighted sum method is used to transform this multi-objective optimization problem into a single-objective optimization problem. The battery lifetime is the most important objective, and the weights are set as $\lambda_1 = 0.5$, $\lambda_2 = 0.1$, $\lambda_3 = 0.2$, and $\lambda_4 = 0.2$. Based on the performance and structure requirements obtained from the multidisciplinary analysis, the constraints are provided as follows:

$$\begin{cases} g_1 = P_F - 3 \\ g_2 = \Delta T - 30 \\ g_3 = \Delta p - 2000 \\ g_4 = T_{\max} - 325 \\ g_5 = V - 0.005 \\ g_6 = \dot{q} - 300 \end{cases} \tag{3}$$

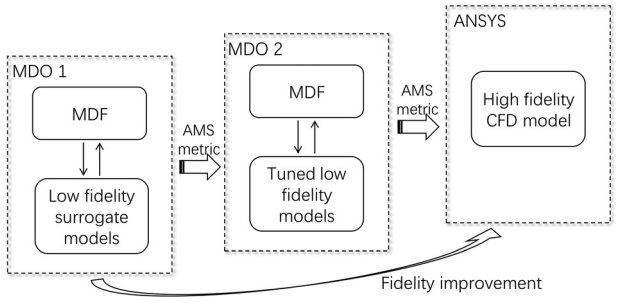

Fig. 8 Variable-fidelity based MDO architecture using MDF

4.2 Variable Fidelity-Based Multidisciplinary Design Optimization Architecture of the Air-Based Battery Thermal Management System. Considering the complexity of the optimization problem, the MDF method [21] is selected to perform the variable fidelity-based MDO of the BTMS in this paper as illustrated in Fig. 8. There are three optimization stages during the whole variable fidelity-based optimization process, including the MDO 1, the MDO 2, and the ANSYS optimization. MDO 1 uses the low fidelity surrogate models as the computing base to perform the optimization and MDO 2 uses the tuned low fidelity models as the computing base. During the variable fidelity-based MDO process, the AMS metric manages the switches between different fidelity models. The final switch from the tuned low fidelity model to the high fidelity CFD model is realized by using the MATLAB scripts to call the ANSYS 17.1.

4.3 Results. Based on multiple numerical experiments, the critical probability p_{cr} in this paper is set to be 0.05. After 24 iterations, the convergence history of the variable fidelity-based MDO is obtained and illustrated in Fig. 9. As seen from Fig. 9(*a*), the convergence curve reaches the optimal solution at the 24th iteration after two switches. Figure 9(*b*) shows that the constraint violation is zero after the 14th iteration. Table 4 lists the initial values of the design variables and the optimal solutions. The final optimal value of the objective function is 0.1699 that is reduced

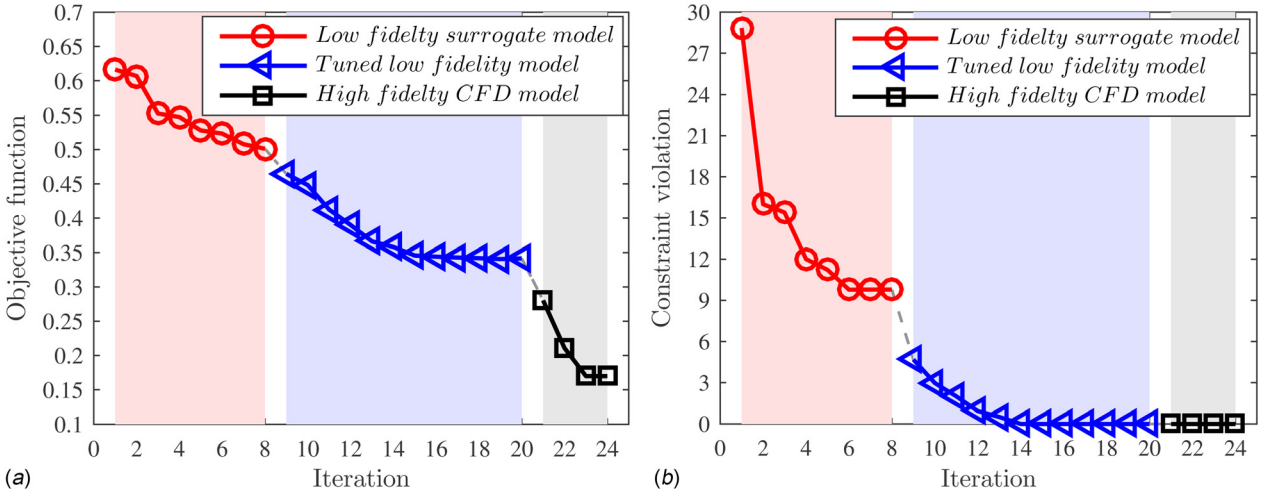

Fig. 9 The convergence history of objective and constraint violation during the variable-fidelity MDO of the BTMS: (*a*) the optimization history of variable-fidelity MDO using MDF and (*b*) the constraint violations history of variable-fidelity MDO using MDF

Table 4 Battery thermal management system optimization results

Design variable (unit)	Initial value	Optimal solution
b_1 (mm)	3.00	2.46
b_2 (mm)	3.00	1.95
b_3 (mm)	3.00	2.88
b_4 (mm)	3.00	2.39
b_5 (mm)	3.00	0.75
b_6 (mm)	3.00	1.74
b_7 (mm)	3.00	0.72
b_8 (mm)	3.00	4.58
b_9 (mm)	3.00	4.11
b_{10} (mm)	3.00	4.96
b_{11} (mm)	3.00	3.98
a_1 (mm)	7.00	8.83
a_2 (mm)	7.00	12.09
a_3 (mm)	7.00	12.82
a_4 (mm)	7.00	14.81
$\dot{m}$ (kg/s)	0.0150	0.0149
$\dot{q}$ (W/m^2)	213.64	203.98
Objective function	0.6162	0.1699

by 72.91% from the initial value 0.6162. The four sub-objectives also achieve the optimal results: $t_{opt} = 9.88$ year, $\Delta T_{opt} = 21.88$ K, $P_{F_{opt}} = 0.85$ W, and $V_{opt} = 0.0032$ m^3. After the MDO process, constraints of the pressure drop Δp, the battery maximum temperature T_{max}, and the heat flux $\dot{q}$ decrease to 51.63 Pa, 315.03 K, and 203.98 W/m^2, respectively.

It is observed from Fig. 9 that the AMS technique adaptively makes the MDO process of the BTMS switch twice from lower to higher level of fidelity in the entire phase. It is found that the tuned low fidelity phase experiences the maximum number of iterations, while the high fidelity CFD phase experiences the minimum number of iterations. Most of the optimization iterations locate in the first two surrogated phases, which cuts off the unnecessary iterations needed by the final CFD simulation. Therefore, the total optimization time is dramatically reduced. The computational time of the low fidelity surrogate model stage and the tuned low fidelity model stage are 43.57 s and 59.63 s, respectively, (Windows 10 system with 6 1.60 GHz Intel® Xeon™ processors and 32.0 GB of RAM memory, located in Richardson, TX). For the high fidelity CFD model stage, the computational time is approximately 2 h.

Figures 10(*a*) and 10(*b*) illustrate how the AMS metric is identified at every optimization iteration and when/where the MDO process switches to the next higher level of fidelity models at the 8th optimization iteration and the 20th optimization iteration. The characters "ⓘ" denote the AMS metric identification conducted at the *i*th optimization iteration. The solid curves are the

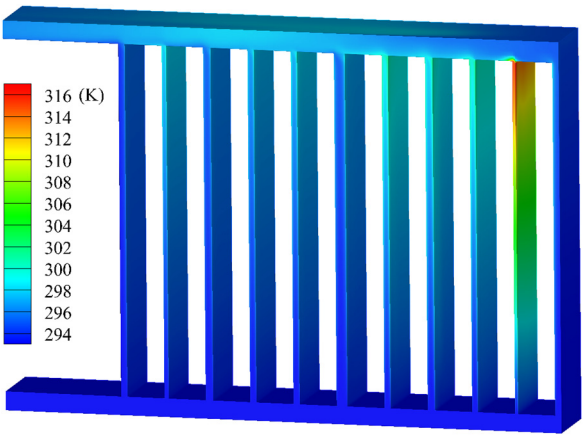

Fig. 11 The temperature distribution of the final optimal solution using AMS-based variable-fidelity MDO

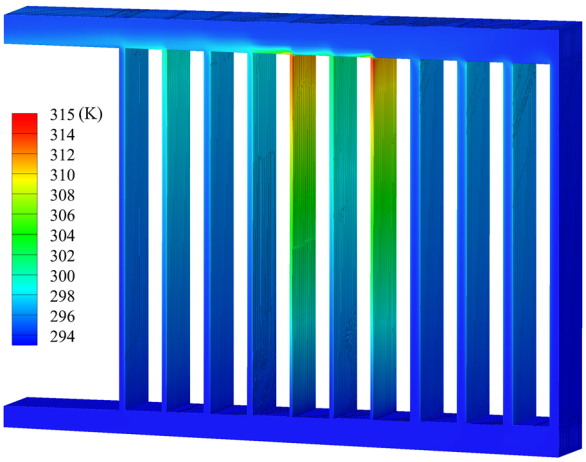

Fig. 12 The temperature distribution of the final optimal solution using Co-Kriging-based variable-fidelity MDO

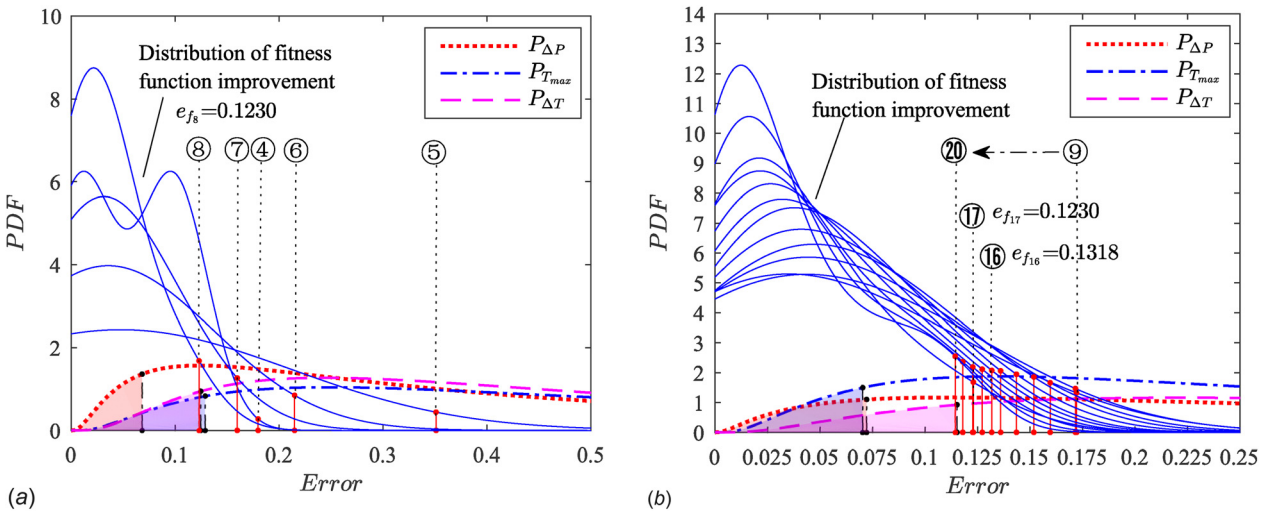

Fig. 10 Identification history during the variable-fidelity MDO of the BTMS: (*a*) identification history in the phase of the low fidelity models and (*b*) identification history in the phase of the tuned low fidelity models

Table 5 The comparison of the AMS and Co-Kriging-based variable-fidelity MDO for BTMS

Variable-fidelity MDO	Objective	t_{opt} (year)	ΔT_{opt} (K)	$P_{F_{opt}}$ (W)	V_{opt} (m^3)	Δp (Pa)	T_{max} (K)	$\dot{q}$ (W/m^2)
Co-Kriging based	0.2154	8.36	23.48	1.50	0.0033	200.13	316.63	202.21
AMS based	0.1699	9.88	21.88	0.85	0.0032	51.63	315.03	203.98
Improvement	−21.12%	+18.18%	−6.81%	−43.33%	−3.03%	−74.20%	−0.51%	+0.88%

Notice: "+" means increase; "−" means decrease.

distributions of fitness function improvement in every optimization iteration. The corresponding vertical straight line sections, which are one-to-one correspondence with the characters "ⓘ" are the cut-off values in the distributions of fitness function improvement. Due to the minimum dimension limitation of the input array used by kernel density estimation, the first identification of the AMS metric is conducted at the 4th optimization iteration, followed by the subsequent identifications as shown in Fig. 10(*a*). It is observed that the first AMS metric identification (at the 4th optimization iteration) can be taken as a "queue-jumper" among the identifications occurring in the phase of the low fidelity surrogate models. The reason of this phenomenon is that the fitness function improvement Δf_3 obtained from the 2nd and 3rd iterations ($\Delta f_3 = (f_3 - f_2)/f_3$) tends to be very large, as show in Fig. 9(*a*). A more accurate distribution is obtained because a large number of points are available for kernel density estimation. By comparing Figs. 10(*a*) and 10(*b*), the cut-off value at the 8th optimization iteration is smaller than that at the 9th optimization iteration, or even smaller than the 16th optimization iteration. It is because that the fitness function improvements are relatively large in the early stage after the MDO process switches to the tuned low fidelity models, as illustrated from Fig. 9(*a*). With the fitness function improvements becoming smaller, the AMS metric is satisfied quickly at the 20th optimization iteration and the MDO process switches to the high fidelity CFD model. Then the optimization process experiences four iterations, and the final optimal CFD optimization results are obtained. The final temperature distribution is shown in Fig. 11. The results show that the performance of the lithium-ion battery is greatly improved, especially the battery lifetime.

To further demonstrate the merits of the proposed method in terms of efficiency and accuracy, a Co-Kriging-based variable-fidelity MDO is also performed. The Co-Kriging surrogate models are developed based on the same 200 high-fidelity CFD simulations (with fine mesh) and additional 200 low-fidelity CFD simulations (with coarse mesh). The Co-Kriging-based optimization results are verified using CFD simulations as illustrated in Fig. 12. The comparison between the AMS-based and Co-Kriging-based variable-fidelity MDO is listed in Table 5. It is seen that, by using the AMS-based variable-fidelity MDO, the objective function is decreased by 21.12% from 0.2154 that is obtained by the Co-Kriging-based method. The battery maximum temperature T_{max} of the Co-Kriging-based variable-fidelity MDO is 321.16 K, which is higher than that obtained using the AMS-based variable-fidelity MDO. For the battery lifetime, the AMS-based variable-fidelity MDO also produces a longer lifetime than that obtained from the Co-Kriging-based variable-fidelity MDO. Overall, the proposed variable-fidelity MDO has shown better performance than the Co-Kriging-based variable-fidelity method.

5 Conclusion

A variable fidelity-based MDO of an air-based BTMS in electric vehicles was developed in this paper. Based on the multidisciplinary analysis, four major subsystems in terms of their respective disciplines are taken into account, including the thermodynamics, the fluid dynamics, the structure, and the battery lifetime. Aiming to perform the variable fidelity-based MDO, three low fidelity surrogate models and three tuned low fidelity models were established to represent the corresponding subsystem performance metrics. The variable fidelity-based MDO architecture was established and the AMS technique was adopted to conduct the model switching during the optimization. By setting the MDO objectives to maximize the battery lifetime and minimize the battery cells temperature difference, fan power, and battery volume, the 17 design parameters (including 11 passage spacing sizes, 4 manifold sizes, heat flux, and mass flow rate) were optimized. The results of the variable fidelity-based MDO showed that the variable-fidelity MDO can balance the characteristics of the pure mathematical models and the expensive computational simulations, thereby finding the optimal solutions efficiently and accurately. The lifetime of the battery module was significantly improved by reducing the temperature difference and battery volume.

Different types of uncertainties may present in such a complex system, such as the uncertainty in the manufacturing process and the uncertainty in the passage spacing size during the assembly process. Therefore, an uncertainty analysis of the BTMS could further improve the thermal and reliability performance, which could be a significant extension for the future work.

Acknowledgment

This work is supported by the University of Texas at Dallas. Xiaobang Wang is supported by the China Scholarship Council.

References

[1] Park, H., 2013, "A Design of Air Flow Configuration for Cooling Lithium Ion Battery in Hybrid Electric Vehicles," J. Power Sources, **239**, pp. 30–36.
[2] Xun, J., Liu, R., and Jiao, K., 2013, "Numerical and Analytical Modeling of Lithium Ion Battery Thermal Behaviors With Different Cooling Designs," J. Power Sources, **233**, pp. 47–61.
[3] Sun, H., and Dixon, R., 2014, "Development of Cooling Strategy for an Air Cooled Lithium-Ion Battery Pack," J. Power Sources, **272**, pp. 404–414.
[4] Mohammadian, S. K., and Zhang, Y., 2015, "Thermal Management Optimization of an Air-Cooled Li-Ion Battery Module Using Pin-Fin Heat Sinks for Hybrid Electric Vehicles," J. Power Sources, **273**, pp. 431–439.
[5] Uddin, A. I., and Ku, J., 2015, "Design and Simulation of Lithium-Ion Battery Thermal Management System for Mild Hybrid Vehicle Application," SAE Paper No. 2015-01-1230.
[6] Dandurand, B., Guarneri, P., Fadel, G., and Wiecek, M. M., 2013, "Equitable Multi-Objective Optimization Applied to the Design of a Hybrid Electric Vehicle Battery," ASME J. Mech. Des., **135**(4), p. 041004.
[7] Mejía-Rodríguez, G., Renaud, J. E., and Tomar, V., 2008, "A Variable Fidelity Model Management Framework for Designing Multiphase Materials," ASME J. Mech. Des., **130**(9), p. 091702.
[8] Xiong, Y., Chen, W., and Tsui, K.-L., 2008, "A New Variable-Fidelity Optimization Framework Based on Model Fusion and Objective-Oriented Sequential Sampling," ASME J. Mech. Des., **130**(11), p. 111401.
[9] Yamazaki, W., and Mavriplis, D. J., 2012, "Derivative-Enhanced Variable Fidelity Surrogate Modeling for Aerodynamic Functions," AIAA J., **51**(1), pp. 126–137.
[10] Réthoré, P.-E., Fuglsang, P., Larsen, G. C., Buhl, T., Larsen, T. J., and Madsen, H. A., 2011, "Topfarm: Multi-Fidelity Optimization of Offshore Wind Farm," 21st International Offshore and Polar Engineering Conference, Maui, HI, June 19–24.
[11] Tarkian, M., Persson, J., Ölvander, J., and Feng, X., 2012, "Multidisciplinary Design Optimization of Modular Industrial Robots by Utilizing High Level Cad Templates," ASME J. Mech. Des., **134**(12), p. 124502.
[12] Brezillon, J., Carrier, G., and Laban, M., 2011, "Multidisciplinary Optimization of Supersonic Aircraft Including Low-Boom Considerations," ASME J. Mech. Des., **133**(10), p. 105001.
[13] Mehmani, A., Chowdhury, S., Tong, W., and Messac, A., 2015, "Adaptive Switching of Variable-Fidelity Models in Population-Based Optimization,"

Engineering and Applied Sciences Optimization, Springer, Cham, Switzerland, pp. 175–205.
[14] Jones, D. R., Schonlau, M., and Welch, W. J., 1998, "Efficient Global Optimization of Expensive Black-Box Functions," J. Global Optim., **13**(4), pp. 455–492.
[15] Rodriguez, J., Perez, V., and Renaud, J., 2001, "Sequential Approximate Optimization Using Variable Fidelity Response Surface Approximations," AIAA Paper No. 2000-1391.
[16] Mehmani, A., Chowdhury, S., and Messac, A., 2015, "Predictive Quantification of Surrogate Model Fidelity Based on Modal Variations With Sample Density," Struct. Multidiscip. Optim., **52**(2), pp. 353–373.
[17] Wang, X., Li, M., Liu, Y., Sun, W., Song, X., and Zhang, J., 2017, "Surrogate Based Multidisciplinary Design Optimization of Lithium-Ion Battery Thermal Management System in Electric Vehicles," Struct. Multidiscip. Optim., **56**(6), pp. 1555–1570.
[18] Sobol', I. M., 1967, "On the Distribution of Points in a Cube and the Approximate Evaluation of Integrals," Zh. Vychisl. Mat. Mat. Fiz., **7**(4), pp. 784–802.
[19] Zadeh, P. M., Toropov, V. V., and Wood, A. S., 2009, "Metamodel-Based Collaborative Optimization Framework," Struct. Multidiscip. Optim., **38**(2), pp. 103–115.
[20] Haftka, R. T., 1991, "Combining Global and Local Approximations," AIAA J., **29**(9), pp. 1523–1525.
[21] Cramer, E. J., Dennis, J., Jr., Frank, P. D., Lewis, R. M., and Shubin, G. R., 1994, "Problem Formulation for Multidisciplinary Optimization," SIAM J. Optim., **4**(4), pp. 754–776.